Neutron inelastic cross-section measurements for ^{24}Mg

A. Olacel,[1,2,*] C. Borcea,[1] P. Dessagne,[3] M. Kerveno,[3] A. Negret,[1] and A. J. M. Plompen[4]
[1]*Horia Hulubei National Institute for Physics and Nuclear Engineering, Reactorului 30, 077125 Bucharest-Măgurele, Romania*
[2]*University of Bucharest, Faculty of Physics, Atomistilor 405, 077125, Bucharest-Măgurele, Romania*
[3]*CNRS, Université de Strasbourg, UMR7178, IPHC, 23 rue du Loess 67037 Strasbourg, France*
[4]*European Commission, Joint Research Center, Institute for Reference Materials and Measurements, B-2440 Geel, Belgium*
(Received 24 June 2014; published 8 September 2014)

The γ production cross sections from neutron inelastic scattering on ^{24}Mg were measured for neutron energies up to 18 MeV at GELINA (the Geel Linear Accelerator), the neutron source operated by EC-JRC-IRMM, Belgium. The level cross section and the total inelastic cross section were determined. We used the GAINS (Gamma Array for Inelastic Neutron Scattering) spectrometer with seven large-volume high-purity germanium (HPGe) detectors placed at 110° and 150° with respect to the beam direction. The neutron flux was determined with a ^{235}U fission chamber. The results are compared with calculations performed with the TALYS 1.6 code using the default settings.

DOI: 10.1103/PhysRevC.90.034603 PACS number(s): 25.40.Fq, 27.30.+t, 29.30.Kv

I. INTRODUCTION

The history of the last century shows that energy consumption is proportional to economic development. As the world's energy sources are running low, nuclear energy becomes an attractive type of energy, even if it has to face extremely delicate issues such as safety, nuclear waste, proliferation, cost efficiency, etc. The next generation of nuclear reactors (generation IV) are currently being developed. They make better use of resources and minimize the high-level waste output by recycling fuel and minor actinides. However, their design requires a better understanding of all neutron-induced reactions that may occur during operation. Numerous studies, based on complex simulation codes, show that, in order to keep risks within acceptable limits, precise nuclear data are required [1,2].

Magnesium represents a major ingredient of alloy steel which constitutes a common structural material in the design of nuclear reactors. Magnesium is also a component of CERCER [an alloy of a ceramic magnesia (MgO) matrix with incorporated mixed actinide dioxide fuel particles containing minor actinides (MAs)], one of the composite fuels selected for transmutation of MAs in the European Facility for Industrial Transmutation (EFIT) [3]. EFIT is an accelerator driven system (ADS) with a subcritical core loaded with dedicated fuels and cooled by liquid lead. The subcritical core receives neutrons from a lead spallation neutron source, driven by the proton beam of a linear accelerator (LINAC). The selection and optimization of the dedicated fuel for EFIT is an important task. The fuel has to ensure high minor actinides transmutation efficiency and achieve high MA burn-up to be economically acceptable. At an earlier stage of the EUROTRANS project, two composite fuel systems were selected as the most promising candidates for detailed studies and optimization: CERCER and CERMET [containing the same type of oxide fuel particles in a metallic molybdenum (Mo) matrix] [4].

The SFR (sodium-cooled fast reactor) is a generation IV reactor designed for—among other reasons—management of high-level wastes and, in particular, management of plutonium and other actinides [5]. One of its risks is the activation of ^{23}Na; ^{24}Na results from the capture of neutrons on ^{23}Na, and decays with a half-life of $\approx$15 hours causing small accumulations of ^{24}Mg in the reactor that should be considered when the criticality factor is evaluated.

Therefore, a good knowledge of the neutron-induced reactions on ^{24}Mg becomes mandatory for the design of the generation IV reactors.

Neutron inelastic scattering experiments were performed in the 1970s by Kinney *et al.* [6] and Dickens *et al.* [7] at Oak Ridge National Laboratory (ORNL), USA. The first of them reported cross sections of natural magnesium for inelastic scattering of neutrons in the energy range from 4.19 to 8.56 MeV, while the second extended the neutron energy range from 0.8 to 20 MeV.

More recently, Korzh *et al.* [8] performed a neutron inelastic scattering experiment on ^{24}Mg in order to study the cross sections of fast neutron scattering by magnesium nuclei. The magnesium sample was a full cylinder with 3.0 cm diameter and 4.0 cm height. The experiment was performed at a Van de Graaff facility; the neutron flux was monitored with a stilbene detector with pulsed shape discrimination and with a long counter. The total neutron energy resolution varied from (30–100) keV at 1–3 MeV to (90–150) keV at 5–7 MeV. The total inelastic cross section for six points in the 2–7 MeV energy range were determined, yielding a maximum value around 0.5 b at 5 MeV.

Based on our extended experience in the field of neutron inelastic cross section measurements (see [9–13]) we performed an experiment aiming to improve significantly the knowledge of the cross sections on ^{24}Mg . The next two sections present the experimental setup and the analysis technique, while the fourth one presents the results together with theoretical discussion based on calculations performed with the TALYS 1.6 reaction code [14].

*aolacel@tandem.nipne.ro

II. THE EXPERIMENTAL SETUP

The time of flight (ToF) facility GELINA (the Geel Linear Accelerator) has been specifically designed and built for high-resolution cross section measurements. It is a multi-user facility, serving up to 12 different experiments simultaneously, and providing a pulsed white neutron source with neutron energies up to ≈20 MeV. Among the pulsed white spectrum neutron sources available in the world, GELINA has the best time resolution [15]. GELINA combines four units: a linear electron accelerator delivering a pulsed electron beam, a compression magnet, a rotary mercury-cooled uranium target, and 12 flight paths ranging from 10 to 400 m.

Electrons are accelerated to energies in the range of 70–140 MeV with a repetition rate of 800 Hz and a full width at half maximum of the pulse of less than 1 ns. The electrons produce bremsstrahlung in a rotating depleted uranium target. The neutrons are produced through U(γ,xn) and U(γ, fission) reactions. The facility is described in more detail in Refs. [15,16].

The current measurement was performed in a station located 200 m from the neutron source. The neutron flux was monitored with a ^{235}U FC (fission chamber) placed in the measurement station [17]. In the cabin the neutron beam was collimated to a diameter of 61 mm and the energy-integrated flux was about 500 n/cm^2 s. To avoid moderated neutrons and to attenuate the γ flash proceeding the neutron pulses two filters were used, one of ^{10}B (1.23 g/cm^2) and one of $^{\text{nat}}$U (36.8 g/cm^2), both placed in the middle of the source-sample distance.

The GAINS (Gamma Array for Inelastic Neutron Scattering) [18,19] setup was developed with the purpose of measuring high resolution neutron inelastic scattering cross sections using the (n,$n'\gamma$) technique [20].

For this measurement GAINS consisted of eight large-volume high-purity germanium (HPGe) detectors (only seven of them were active during the current measurement) placed at 110° and 150° with respect to the beam direction, with four detectors at each angle, and at distances of 14–16.5 cm from the target. These angles allow an accurate integration of the angular distribution including the sixth order of Legendre polynomials [cos(110°) and cos(150°) are the nodes of the fourth-degree Legendre polynomials]. The detectors have a typical γ energy resolution of 2.3 keV for the 1332 keV peak of ^{60}Co and 100% relative efficiency [19].

The HPGe detectors are read out by DC440 Aquiris digitizers running at 420*10^6 samples/s, with 12-bit amplitude resolution [19]. The waveforms are transferred to PCs and the signal processing is performed online by the data acquisition software that was developed in house. For each signal we are recording the time and the amplitude. The time is related to the energy of the neutron that produced the reaction, while the amplitude is proportional to the γ energy. A neutron energy resolution of ≈1 keV at 1 MeV and up to ≈ 35 keV at 10 MeV is obtained [13].

The ^{24}Mg sample had a diameter of 8.003 ± 0.001 cm and an area density of 0.698 ± 0.001 g/cm^2, and it was irradiated at a distance of 19 868.4 cm from the neutron source.

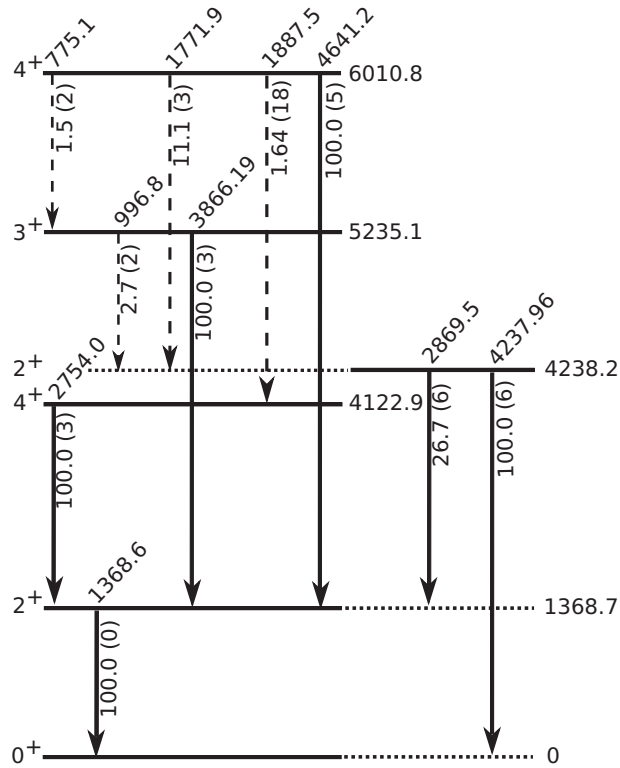

FIG. 1. Low excitation energy level scheme of ^{24}Mg from the evaluated database [22]. The γ transitions marked with continuous lines were observed in the experiment and their production cross section were measured.

III. DATA ANALYSIS

A detailed description of the data analysis procedure is presented in Ref. [21] with an important correction for the flux determination described in Refs. [9,17]. The first step is the identification of the γ transitions based on their energy. As displayed in Fig. 1, six γ transitions from ^{24}Mg were identified.

For those six γ transitions observed in the experiment we calculated the differential γ production cross sections at θ_i = 110° and 150° using

$$\frac{d\sigma_j}{d\Omega}(\theta_i, E_k) = \frac{1}{4\pi}\frac{Y_j(E_k)}{Y_{\text{FC}\,j}(E_k)}\frac{\epsilon_{\text{FC}}\sigma_U(E_k)}{\epsilon_j}\frac{t_U}{t_s}\frac{A_s}{A_U}\frac{1}{c_{ms}(E_k)}, \tag{1}$$

where Y_j is the yield of detector j, $Y_{\text{FC}\,j}$ the FC yield corresponding to detector j, ϵ_{FC} the FC efficiency, ϵ_j the γ efficiency of detector j, σ_U the ^{235}U(n,F) cross section, t_U the thickness of the ^{235}U deposit, t_s the sample thickness, A_U = 235.04 and A_s = 23.98 the atomic mass numbers, and c_{ms} the multiple scattering correction factor.

In order to determine the γ production cross section for each transition we integrated the cross section numerically based on the differential cross section values at 110° and 150°

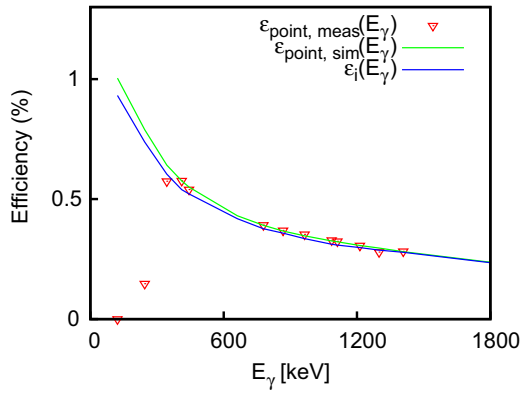

FIG. 2. (Color online) The experimental and simulated (MCNP) efficiency using the point-like source, and the extended (MCNP) efficiency

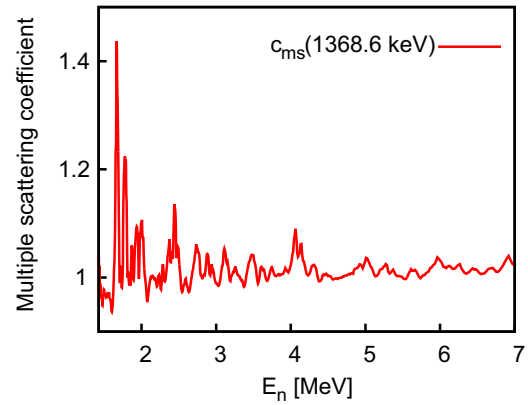

FIG. 3. (Color online) The multiple scattering correction factor for the 1368.6 keV transition.

using the following expression:

$$\sigma(E_k) = 2\pi \left[w_{110^\circ} \frac{d\sigma}{d\Omega}(110^\circ, E_k) + w_{150^\circ} \frac{d\sigma}{d\Omega}(150^\circ, E_k) \right], \quad (2)$$

where E_k is the neutron energy for the bin k, and $\frac{d\sigma}{d\Omega}(110^\circ, E_k)$ and $\frac{d\sigma}{d\Omega}(150^\circ, E_k)$ are the differential γ production cross sections. The angle integration coefficients are $w_{110^\circ} = 1.30429$ and $w_{150^\circ} = 0.69571$. Using the level scheme (Fig. 1) we calculated the level production cross section based on the feeding and the decay of each level. The total inelastic cross section was calculated as a sum of the γ production cross sections of the two transitions feeding directly the ground state [21].

The detection efficiency of the γ rays emitted from the sample (thick, extended source), and the multiple scattering corrections were performed using MCNP5 simulations [23]. The determination of the setup efficiency was performed by a method combining calibration measurements and MCNP5 simulations [24]. The calibration measurements were taken with a point-like ^{152}Eu source. The activity of the calibration source was (18.9 ± 0.6) kBq and this induced in the detectors a counting rate similar to the one produced by the neutron-induced reaction. A geometrical model of the setup was developed in MCNP. The source was placed in the position of the Mg sample and the experimental efficiencies for the point-like source were simulated. The geometrical model was adjusted to reproduce the calibration data and was considered validated when the simulated efficiencies $\epsilon_{\text{point, sim}}(E_\gamma)$ for the ^{152}Eu source overlapped with the experimental measured efficiencies $\epsilon_{\text{point, meas}}(E_\gamma)$. In order to determine the efficiencies of the detectors for the actual measurements, we replaced the point source in the model with an extended one reproducing the geometrical details and the composition of the ^{24}Mg sample.

Figure 2 displays the experimental and simulated (MCNP) efficiencies using the point-like source, and the experimental efficiency for the extended sample $\epsilon_i(E_\gamma)$ for one of the detectors.

A second set of simulations was performed in order to determine the multiple scattering correction factor c_{ms}. If a neutron scatters twice in the sample, the effective flux is increased and the time of the $(n,n'\gamma)$ subsequent event no longer corresponds to the energy of the incident neutron. The multiple scattering correction factor calculated for the 1368.6 keV γ ray using MCNP5 is displayed in Fig. 3. The factor is high when the cross section is low. In that case the energy loss following a scattering event results in a substantial increase in the probability for inelastic scattering for the second-chance scatter.

The detailed technique for the determination of the fission chamber efficiency is explained in Ref. [9,17]. The distribution of a typical amplitude spectrum of the fission chamber shows a sharp peak from the alpha decay of ^{235}U at low pulse heights, and the contribution of ^{235}U(n,F) events. The alpha and fission fragment peaks are separated by a plateau, where a software threshold is applied to reject the low-amplitude alpha events. In order to calculate the total number of fissions, the plateau is extrapolated to zero pulse height. The total number of the neutron-induced fission fragments is then calculated from the yield of the fission events above the threshold corrected for the polarity effect of the chamber [17], the number of the fission fragments that stop in the deposits [25], and the inhomogeneity of the UF_4 foils [26]. For the threshold used in this measurement the efficiency of the fission chamber was 84(2)%.

The uncertainties of the parameters used in all the cross section calculations were calculated by the usual quadratic error propagation. The final uncertainties of the cross sections include all the uncertainty components.

IV. RESULTS AND DISCUSSION

^{24}Mg is one of the lightest nuclei investigated up to now at GAINS. This represents a challenge because of the low level density of the nucleus and consequently of the high energy of the emitted γ rays (see Fig. 1). As already mentioned, we were able to detect six γ rays (Table I). For those, we determined the angle integrated γ production cross sections. The production cross sections for the first five excited levels and the total inelastic cross section were calculated using the evaluated level scheme [22].

TABLE I. Examined γ's from ^{24}Mg$(n,n'\gamma)$ and associated initial and final levels [22].

E_γ (keV)	E_{init} (keV)	$^{\text{init}}J_\pi$	E_{final} (keV)	$^{\text{final}}J_\pi$	I_γ	Multipolarity
1368.6	1368.7	2^+	0	0^+	100	$E2$
2754.0	4122.9	4^+	1368.7	2^+	100	$E2$
4238.0	4238.2	2^+	0	0^+	100 (6)	$E2$
2869.5	4238.2	2^+	1368.7	2^+	26.7 (6)	$M1+E2$
3866.2	5235.1	3^+	1368.7	2^+	100 (3)	$M1+E2$
4641.2	6010.8	4^+	1368.7	2^+	100 (5)	$M1+E2$

A. Model calculations

Nuclear model calculations were performed with the TALYS 1.6 [14] code. TALYS is used for the prediction of nuclear reactions involving neutrons, photons, protons, deuterons, tritons, ^{3}He, and alpha particles, in the energy range from 1 keV to 200 MeV and for target nuclides of mass 12 and heavier. TALYS computes the binary reaction models (optical model potentials plus direct reactions), the Hauser-Feshbach models, and the multiple preequilibria for all residual nuclei and particles. For all the models, several parameter sets may be selected which have been obtained from global optimizations of semiempirical and microscopic descriptions. Two calculations with the TALYS code were performed.

The first calculation involves the TALYS default semiempirical model with parameters obtained from global optimizations. The default optical model potentials are the local and global parametrizations of Koning and Delaroche [27]. The level densities are described in the Gilbert and Cameron approach [28] with the constant temperature model at low excitation energies and the backshifted Fermi gas model with an energy dependent level density parameter a accounting for the damped shell effect proposed by Ignatyuk *et al.* [29] at high energies. The relevant values of the level density parameters used in TALYS 1.6 are given in Table II. The γ ray strength functions are described using the Brink-Axel option for all transition types other than $E1$, while for the $E1$ radiation the option used is the generalized Lorentzian form of Kopecky and Uhl [30]. For the first 20 excited levels in the target and residual nuclei, TALYS relies on a nuclear structure and decay table to describe the deexcitation of the nuclei. This table is derived from the Reference Input Parameter Library [31].

A second calculation was performed with the semimicroscopic nucleon-nucleus spherical optical model potential as described in Ref. [32]. The microscopic optical model is that of Bauge *et al.* [33] which was obtained from nuclear densities and the Jeukenne-Lejeune-Mahaux optical model potential for nuclear matter with a folding model in the local density approximation. This model produces good predictions in the mass range from 30 to 240 amu and for energies ranging from 10 keV up to 200 MeV. The low and high energy regimes of the nuclear matter optical model were merged, and energy dependent renormalizations were applied to the potential depth by comparison with experimental data. The level densities are based on the microscopic combinatorial model proposed by Hilaire and Goriely [34] which includes a detailed microscopic calculation of the intrinsic state density and collective enhancement using the nuclear structure properties determined within the deformed Skyrme-Hartree-Fock-Bogoliubov framework. The γ-ray strength functions calculated in the Hartree-Fock-Bogoliubov approach were also taken from the Reference Input Parameter Library.

The two TALYS calculations were compared and no difference was observed.

B. γ production, level and total inelastic cross sections

Our γ production cross sections are compared in Fig. 4 with the default theoretical calculation performed with the TALYS 1.6 code. The calculation describes fairly well the energy average behavior of the cross sections for the 1368.6, 2869.5, 3866.2, and 4238.0 keV transitions (see Figs. 4(a) and 4(c)–4(e)]. The code underestimates the experimental data for the 4641.2 keV transition in the range $E_n \approx 7$–9 MeV [see Fig. 4(f)], but overestimates the 2754.0 keV transition [see Fig. 4(b)]. However, the TALYS 1.6 calculations show a good overall description of the γ production cross section measured in the present work.

Table III displays the formulas used in order to calculate the level cross sections as a function of the γ production cross sections $\sigma^{\gamma}_{E_\gamma}(E_n)$ and the neutron energy ranges where they apply. For each case the lower limit of the range corresponds to the neutron energy threshold for the excitation of the level. The upper limit corresponds to the energy threshold for the excitation of the lowest state that decays to the level of interest through a γ ray undetected by us. Beyond this range the

TABLE II. The default level density parameters used in the TALYS 1.6 code. The level density parameters a at the separation energy (S_n), shell correction energy δW, temperature T, backshift energy E_0, pairing energy Δ, matching energy $^{\text{match}}E_x$, and the calculated and experimental s-wave spacing D_0 are given.

Nuclide	$a(S_n)$ (MeV^{-1})	δW (MeV)	T	E_0 (MeV)	Δ (MeV)	$^{\text{match}}E_x$ (MeV)	D_0 (keV)	$^{\text{exp}}D_0$ (keV)
^{24}Mg	3.24	−2.71	2.27	2.38	4.89	20.83	17.97	
^{25}Mg	3.67	−1.35	2.10	−0.99	2.40	16.26	47±12	47±14

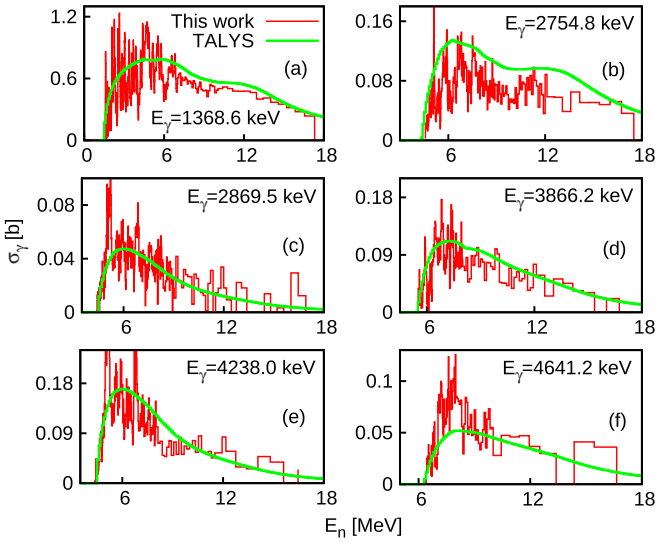

FIG. 4. (Color online) Integrated γ production cross section for each observed transition. The red line represents the results of the present experiment while the green line displays the results of the TALYS 1.6 theoretical calculations using the default input parameters.

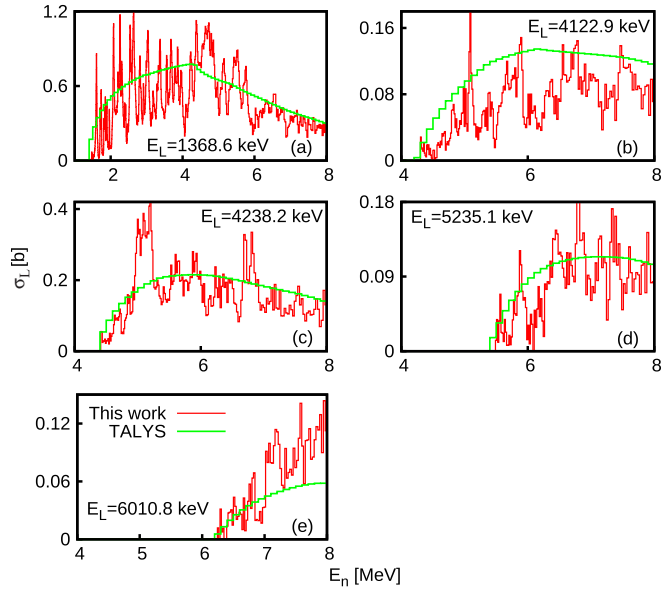

FIG. 5. (Color online) The production cross section for the first five excited levels compared with the TALYS 1.6 default calculations.

values we calculate constitute only lower limits of the level cross sections. Figure 5 displays the production cross sections of the first five excited levels compared with the TALYS 1.6 calculation.

Again, TALYS 1.6 estimates using default parameters reproduce correctly most of the experimental values. As expected from the γ production cross sections, the levels at 4122.9 and 6010.8 keV (decaying through 2754.0 and 4641.2 keV respectively) are in slightly less good agreement with our data [see Figs. 5(b) and 5(e)]. The calculation describes well the experimental data below 8 MeV.

The total inelastic cross section shown in Fig. 6(b) was calculated as a sum of the γ production cross sections of the two transitions feeding directly the ground state (1368.6 and 4238.0 keV). Other γ rays of higher energies that may feed the ground state were not detected with our setup. According to the adopted level scheme [22], the next excited level above the 6010.8 keV that decays directly to the ground state is at 7349.1 keV. This means that the total inelastic cross section determined here is accurate for neutron energy up to 7658.1 keV which is the threshold for exciting the 7349.1-keV level. If the neutron energy is above this value, our cross section should be considered as a lower limit.

Figure 6(b) compares the total inelastic cross section determined in the present experiment with the experimental results of Korzh *et al.* from Ref. [8], the theoretical predictions of the TALYS 1.6 code using the default parameters, and the values from the ENDF/B-VII.1 [35] evaluation. We note that the JEFF-3.1.2 [36] evaluation is identical to ENDF/B-VII.1.

The total inelastic cross section starts to grow at $E_n =$ 1.426 MeV. Resonance structures can be seen until $E_n \approx$ 7–8 MeV. Two deepenings are visible around $E_n = 4$ and 6 MeV, then the total inelastic cross section decreases towards 18 MeV. The cross section reaches a maximum of 1.2 b at $E_n = 4.7$ MeV.

At low energies (up to 3 MeV) the first three points of Korzh *et al.* [8] are in a good agreement with our results, while at energies above 4 MeV our cross sections are clearly higher. The evaluated data from ENDF/B-VII.1 and JEFF-3.1.2 display even higher values. The TALYS 1.6 calculation overlaps with the existing evaluations up to about 7 MeV. As already mentioned,

TABLE III. The formulas used in order to calculate the level cross section as a function of the γ production cross section, and the neutron energy ranges where they apply. The coefficients representing the contributing weights of the observed γ's to the construction of the level cross sections are based on the feeding and the decay of each level.

Level (keV)	Formula	Range (keV)
1368.7	$\sigma^{\gamma}_{1369}(E_n) - \sigma^{\gamma}_{2755}(E_n) - \sigma^{\gamma}_{2870}(E_n) - \sigma^{\gamma}_{3866}(E_n)$-$\sigma^{\gamma}_{4641}(E_n)$	1426.2–6703.0
4122.9	$\sigma^{\gamma}_{2755}(E_n) - 0.0164\sigma^{\gamma}_{4641}(E_n)$	4296.2–7936.7
4238.2	$1.267\sigma^{\gamma}_{4238}(E_n) - 0.027\sigma^{\gamma}_{3866}(E_n) - 0.11\sigma^{\gamma}_{4641}(E_n)$	4416.6–6703.0
5235.1	$1.027\sigma^{\gamma}_{3866}(E_n) - 0.015\sigma^{\gamma}_{4641}(E_n)$	5455.3–7936.8
6010.8	$1.142\sigma^{\gamma}_{4641}(E_n)$	6263.0–8140.7

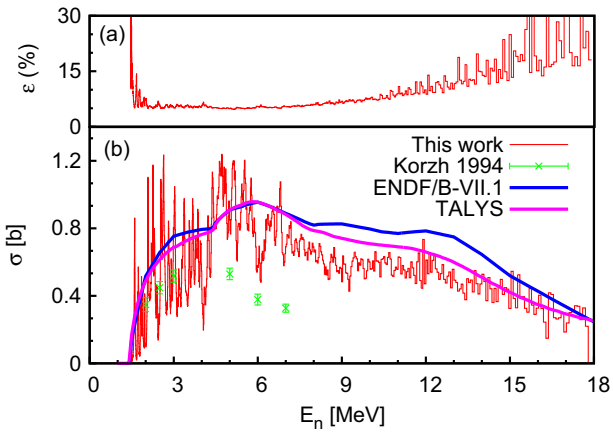

FIG. 6. (Color online) (b) Total inelastic cross section for the ^{24}Mg$(n,n'\gamma)^{24}$Mg reaction. The red line represents the result of our experiment, the green dots the results from the previous experiment of Korzh *et al.* (1994) [8], the dark blue line displays the evaluated values from ENDF/B-VII.1 [35], while the magenta line represents the TALYS 1.6 calculations. (a) The relative total uncertainties.

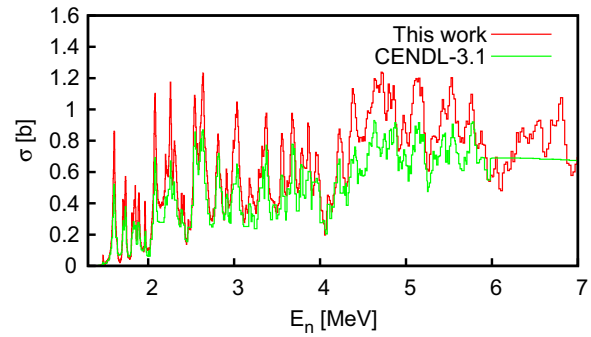

FIG. 7. (Color online) The resonance structure in the inelastic scattering cross section above the threshold. The red line represents our experimental values and the green line the results from CENDL-3.1 evaluation [37]

above $E_n = 7.349$ MeV our result represents a lower limit of the inelastic cross section.

Figure 7 shows a zoom of the total inelastic cross section in comparison with the CENDL-3.1 [37] evaluation, which is the only evaluation displaying the resonant structures at low E_n. This evaluation is based on the differential γ-ray production cross sections measured by Dickens [7] and Clarke [38]. Below 6 MeV the cross sections were calculated assuming that the secondary γ emissions are isotropic, and between 4.3 to 6 MeV the contributions from the second discrete level were included. While our absolute cross sections are higher than CENDL-3.1, the resonant structures are in the same positions.

C. Level densities in the compound nucleus ^{25}Mg

As already mentioned, the very good neutron energy resolution allows us to separate the resonances present in the total inelastic cross section [Fig. 7(b)]. Although a detailed R-matrix fit of the data is beyond the scope of the present article, we performed some simple estimates in order to understand if the resonances represent individual states from the compound nucleus ^{25}Mg or overlap of such states causing fluctuations and resonant structures.

We employed the TALYS 1.6 code to determine which total angular momenta are populated in the compound nucleus during the neutron inelastic scattering on ^{24}Mg. Then we estimated the level densities at the corresponding total angular momenta and excitation energies using the backshifted Fermi gas model (BSFG) following the simple prescription from Refs. [39,40]. The results are compared in Table IV with the experimental level density estimates deduced by direct counting of the resonances from the total inelastic cross section.

We observe that in the neutron energy range from 1.73 to 2.78 MeV, corresponding to the excitation energy in ^{25}Mg around 9.5 MeV, the level density calculated with the BSFG coincides with the number of resonances observed in the total inelastic cross section. As the excitation energy in the compound nucleus increases, this is no longer the case and the two numbers diverge: the calculated level density increases significantly while the number of structures we observe is almost constant. We should also note that our neutron energy resolution deteriorates with energy. We conclude therefore that the resonant structures we observe correspond to individual levels in ^{25}Mg only for very low energies. Already above $E_n = 2.5$–3 MeV these structures represent Ericson fluctuations [41] arising from the overlap of many states from the compound nucleus.

We will finalize this section with a short discussion on the uncertainties. The most important are the systematic errors, because the statistical uncertainties can be reduced by

TABLE IV. Theoretical level densities vs experimental level densities.

E_n range (MeV)	Average E_n (MeV)	$E^*(^{25}\mathrm{Mg})$ (MeV)	$J(^{25}\mathrm{Mg})$ (TALYS)	Theoretical level density (MeV^{-1}) (BSFG)	Experimental level density (MeV^{-1})
1.73–2.78	2.26	9.5	1/2–5/2	19	18
2.78–3.82	3.30	10.5	1/2–7/2	36	18
3.82–4.87	4.34	11.5	1/2–7/2	53	10
4.87–5.91	5.39	12.5	1/2–7/2	79	13
5.91–6.95	6.43	13.5	1/2–9/2	132	11
6.95–7.99	7.47	14.5	1/2–9/2	191	10
7.99–9.03	8.51	15.5	1/2–9/2	275	8

a proper rebinning of the data. The statistical uncertainties of the detector yields were of the order of ≈2% for the strongest transitions. The HPGe efficiency calibration brings an uncertainty of 2%, mainly from the activity of the source and the positioning of the calibration source. The uncertainty of the multiple scattering correction factor calculated from the MCNP5 simulations is smaller than 1%, and the uncertainty of the ^{235}U(n,F) cross section from ENDF/B-VII.1 is 0.7%. The uncertainty of the fission chamber efficiency is 2%. The total resulting uncertainty for the strongest transitions is of the order of 5% [see Fig. 6(a)].

V. CONCLUSIONS

Using a sample of ^{24}Mg, the six most important γ transitions from the neutron inelastic scattering channel were observed. We measured the differential γ production cross section at angles of 150° and 110° in the energy range from threshold energy up to 18 MeV. The angle integrated γ production cross sections were determined in the same energy range.

The total inelastic cross section and the level cross sections were calculated using the low excitation energy level scheme of ^{24}Mg from the evaluated database. For each level up to 6010.8 keV excitation energy at least one γ ray was observed. Above the neutron energy of 7.6 MeV, the total inelastic cross sections presented here represent only lower limits, while the level cross sections are upper limits.

We had a neutron energy resolution of ≈1 keV at 1 MeV and up to ≈35 keV at 10 MeV, and a total uncertainty of 5% for the strongest transitions. The total uncertainty on the γ production cross section of the main transition and on the total inelastic scattering cross section was around 5% up to 7 MeV and less than 15% up to 18 MeV.

In comparison with the previous experiment, the set of cross sections measured in the present experiment have the advantage of covering the full energy range from threshold up to 18 MeV and have a better neutron energy resolution.

In general, the TALYS calculations using the semiempirical default parameters describe well the measured cross sections presented here. The γ production cross sections are described well by the TALYS calculations below about 7.6 MeV. Significant differences with the measured data are visible above this energy. The good agreement of TALYS with the experimental total inelastic cross-section confirms that the compound nucleus and direct reaction modeling, including the associated optical model and level density parameters, is well under control.

ACKNOWLEDGMENTS

The authors thank the technical staff of GELINA (IRMM) for the high-quality beam delivered during the measurements. We also acknowledge D. Bucurescu for useful discussions regarding the level density calculations. This work was partially supported by the Romanian Ministry of Education through Contract No. PN-II-ID-PCE-2011-3-0370 (UEFISCDI). The authors gratefully acknowledge the support of the projects ANDES and CHANDA (European Commission, Seventh Framework Programme EURATOM Contracts No. ANDES FP7-249671 and No. CHANDA FP7-605203). A.O. acknowledges EC-JRC-IRMM for the support offered during her stay in Geel.

[1] G. Aliberti, G. Palmiotti, M. Salvatores, and C. G. Stenberg, Nucl. Sci. Eng. **146**, 13 (2004).

[2] G. Aliberti, G. Palmiotti, and M. Salvatores, in *Proceedings of NEMEA-4 Workshop on Neutron Measurements, Evaluations and Applications, October 16–18, 2007, Prague, Czech Republic*, edited by A. Plompen (Publications Office of the European Union, Luxembourg, 2008), p. 113.

[3] J. U. Knebel, H. Ait Abderrahim, L. Cinotti, F. Delage, C. Fazio, M. Giot, B. Giraud, E. Gonzalez, S. Monti, and A. C. Mueller, in *Proceedings of FISA 2006, EU Research and Training in Reactor Systems, July, 2006, Luxemburg*, edited by G. Van Goethem, P. Manolatos, M. Hugon, V. Bhatnagar, S. Casalta, and M. Deffrennes (Publications Office of the European Union, Luxembourg, 2006), p. 353.

[4] W. Maschek, X. Chen, C. Matzerath Boccaccini, A. Rineiski, V. Sobolev, P. Smith, R. Thetford, J. Wallenius, F. Delage, J.-P. Ottaviani, S. Pillon, and D. Haasin, *Actinide and Fission Product Partitioning and Transmutation: 9th Information Exchange Meeting, September 25-29, 2006, Nimes, France*, NEA No. 6282 (Nuclear Energy Agency, Issy-les-Moulineaux, France, 2007), p. 137.

[5] https://www.gen-4.org.

[6] W. E. Kinney and F. G. Perey, ORNL-TM Report No. 4550, 1970 (unpublished).

[7] J. K. Dickens, T. A. Love, and G. L. Morgan, ORNL-TM Report No. 4544, 1974 (unpublished).

[8] I. A. Korzh, V. A. Mishchenko, N. M. Pravdivy, and N. T. Sklyar, Ukr. Fys. J. **39**, 785 (1994).

[9] C. Rouki, P. Archier, C. Borcea, C. De Saint Jean, J. C. Drohe, S. Kopecky, A. Moens, N. Nankov, A. Negret, G. Noguere, A. J. M. Plompen, and M. Stanoiu, Nucl. Instrum. Methods Phys. Res. **672**, 82 (2012).

[10] A. Negret, C. Borcea, and A. J. M. Plompen, J. Kor. Phys. Soc. **59**, 1765 (2011).

[11] C. Rouki, A. R. Domula, J. C. Drohe, A. J. Koning, A. J. M. Plompen, and K. Zuber, Phys. Rev. C **88**, 054613 (2013).

[12] M. Kerveno *et al.*, Phys. Rev. C **87**, 024609 (2013).

[13] L. C. Mihailescu, C. Borcea, A. J. Koning, and A. J. M. Plompen, Nucl. Phys. A **786**, 1 (2007).

[14] A. J. Koning, S. Hilaire, and M. C. Duijvestijn, in *ND2007, Proceedings of the International Conference on Nuclear Data for Science and Technology, April 22–27, 2007, Nice, France*, edited by O. Berssilon, F. Gunsing, E. Bauge, R. Jacqmin, and S. Leray (EDP Sciences, Les Ulis, France, 2008), p. 211.

[15] D. Ene, C. Borcea, S. Kopecky, W. Mondelaers, A. Negret, and A. J. M. Plompen, Nucl. Instrum. Methods Phys. Res. A **618**, 54 (2010).

[16] M. Flaska, A. Borella, D. Lathouwers, L. C. Mihailescu, W. Mondelaers, A. J. M. Plompen, H. van Dam and T. H. J. J. van der Hagen, Nucl. Instrum. Methods Phys. Res. A **531**, 392 (2004).

[17] A. Plompen, N. Nankov, C. Rouki, M. Stanoiu, C. Borcea, D. Deleanu, A. Negret, P. Dessagne, M. Kerveno, G. Rudolf, J. C. Thiry, M. Mosconi, and R. Nolte, J. Kor. Phys. Soc. **59**, 1581 (2011).
[18] A. Negret, C. Borcea, Ph. Dessagne, M. Kerveno, N. Nankov, A. Olacel, A. J. M. Plompen, and C. Rouki, Nucl. Data Sheets **119**, 179 (2014).
[19] A. Negret, C. Borcea, J. C. Drohe, L. C. Mihailescu, A. J. M. Plompen, and R. Wynants, in *ND2007, Proceedings of the International Conference on Nuclear Data for Science and Technology, April 22–27, 2007, Nice, France*, edited by O. Bersillon, F. Gunsing, E. Bauge, R. Jacqmin, and S. Leray (EDP Sciences, Les Ulis, France, 2008), p. 1015.
[20] A. Negret, C. Borcea, D. Bucurescu, D. Deleanu, Ph. Dessagne, D. Filipescu, D. Ghita, T. Glodariu, M. Kerveno, N. Marginean, R. Marginean, C. Mihai, S. Pascu, A. J. M. Plompen, T. Sava, and L. Stroe, Phys. Rev. C **88**, 034604 (2013).
[21] L. C. Mihailescu, L. Olah, C. Borcea, and A. J. M. Plompen, Nucl. Instrum. Methods Phys. Res. A **531**, 375 (2004).
[22] R. B. Firestone, Nucl. Data Sheets **108**, 2319 (2007).
[23] https://laws.lanl.gov/vhosts/mcnp.lanl.gov and references therein.
[24] D. Deleanu, C. Borcea, Ph. Dessagne, M. Kerveno, A. Negret, A. J. M. Plompen, and J. C. Thiry, Nucl. Instrum. Methods Phys. Res. **624**, 130 (2010).
[25] C. Butz-Jorgensen, H.-H. Knitter, and G. Bortels, Nucl. Instrum. Methods Phys. Res. **236**, 630 (1985).
[26] P. Schillebeeckx, A. Borella, J. C. Drohe, R. Eykens, S. Kopecky, C. Massimi, L. C. Mihailescu, A. Moens, M. Moxon, and R. Wynants, Nucl. Instrum. Methods Phys. Res. A **613**, 378 (2010).
[27] A. Koning and J. Delaroche, Nucl. Phys. A **713**, 231 (2003).
[28] A. Gilbert and A. G. W. Cameron, Can. J. Phys. **43**, 1446 (1965).
[29] A. V. Ignatyuk, G. N. Smirenkin, and A. S. Tishin, Yad. Fiz. **21**, 485 (1975) [Sov. J. Nucl. Phys. **21**, 255 (1975)].
[30] J. Kopecky and M. Uhl, Phys. Rev. C **41**, 1941 (1990).
[31] R. Capote *et al.*, Nucl. Data Sheets **110**, 3107 (2009).
[32] E. Bauge, J. P. Delaroche, and M. Girod, Phys. Rev. C **63**, 024607 (2001).
[33] E. Bauge, J. P. Delaroche, and M. Girod, Phys. Rev. C **58**, 1118 (1998).
[34] S. Goriely, S. Hilaire, and A. J. Koning, Phys. Rev. C **78**, 064307 (2008).
[35] M. B. Chadwick *et al.*, Nucl. Data Sheets **112**, 2887 (2011).
[36] A. Santamarina *et al.*, in *JEFF Report 22*, edited by A. Santamarina, D. Bernard and Y. Rugama (Nuclear Energy Agency, Issy-les-Moulineaux, France, 2009).
[37] Z. G. Ge, Z. X. Zhao, H. H. Xia, Y. X. Zhuang, T. J. Liu, J. S. Zhang, and H. C. Wu, J. Kor. Phys. Soc. **59**, 1052 (2011).
[38] R. L. Clarke and W. G. Cross, Nucl. Phys. **53**, 177 (1964).
[39] T. von Egidy and D. Bucurescu, Phys. Rev. C **72**, 044311 (2005).
[40] T. von Egidy and D. Bucurescu, J. Phys.: Conf. Ser. **338**, 012028 (2012)
[41] T. Ericson, Ann. Phys. (NY) **23**, 390 (1963).